

# A geometric model of growth for cubic crystals: Diamond



Alexander Bogatskiy<sup>a</sup>, James E. Butler<sup>b,c,\*</sup>

<sup>a</sup> Department of Higher Mathematics and Mathematical Physics, Faculty of Physics, Saint-Petersburg State University, Russian Federation

<sup>b</sup> Diamond Electronics Laboratory, Institute of Applied Physics – Nizhny Novgorod, Russian Federation

<sup>c</sup> Dept. of Physics, St. Petersburg Electrotechnical University, Russian Federation

## ARTICLE INFO

### Article history:

Received 5 December 2014

Received in revised form 28 December 2014

Accepted 29 December 2014

Available online 7 January 2015

### Keywords:

Diamond

Twinning

Model

Cubic

Geometric

## ABSTRACT

A mathematical and software implementation of a geometrical model of the morphology of growth in a cubic crystal system, such as diamond, is presented based on the relative growth velocities of four low index crystal planes: {100}, {110}, {111}, and {113}. The model starts from a seed crystal of arbitrary shape bounded by {100}, {110}, {111} and/or {113} planes, or a vicinal (off axis) surface of any of these planes. The model allows for adjustable growth rates, times, and seed crystal sizes. A second implementation of the model nucleates a twinned crystal on a {100} surface and follows the evolution of its morphology. New conditions for the stability of penetration twins on {100} and {111} surfaces in terms of the alpha, beta, and gamma growth parameters are presented.

© 2015 Elsevier B.V. All rights reserved.

## 1. Introduction

Early on in the growth of diamond crystals by chemical vapor deposition (CVD) it was observed that the crystal habit was bounded by the general appearance of several low index planes [1–3]. Four crystal faces with the following Miller indices: {100}, {110}, {111}, {113} were observed under varying growth conditions [4,5]. However, close microscopic examination of these planes often indicated that they were not atomically smooth, but rather displayed steps of various heights. For the purposes of this paper, this ‘roughness’ which is likely to be important to the local stereochemical modeling of the growth chemistry [6,7], will be ignored in order to focus on a model of the more macroscopic growth features. The macroscopic crystal shape observed most often was cubo-octahedral and was described by a parameter, alpha, which is proportional to the growth velocity of the cube face, {100}, to the octahedral face, {111} [8,9]. Only the slowest growing crystal facets are observed and the relative growth rate of each facet depends on complex factors such as the flux of reactive species to the surface, the surface temperature, and surface structure. Hence, depending on the growth conditions, not all facets will be observed at any given time. In 2006, a morphological growth model which included the possibility of the four observed faces, {100}, {110}, {111}, {113}, was introduced which described the crystal growth morphology in terms of three parameters, alpha, beta, and gamma, defined below [10]. The results of this model,

but not the means for computation, have been thoroughly described in multiple subsequent papers [11–15]. The purpose of the present paper is to present a theory behind the implementation of a morphological growth model for diamond (and potentially, other cubic crystals), demonstrate the implementation of the model in readily available software (Wolfram Mathematica), generalize the model to off axis cut surfaces (vicinal) of the initial seed crystal, and to extend the model to demonstrate the morphology of a simple twinned crystal appearing on the {100} face.

Crystal twinning is very commonly observed CVD diamond growth [8,9,16]. Twinning usually occurs on a local {111} plane, and can have the impact of degrading the quality of the material [16–19]. For this reason, the model presented here has been modified to include the nucleation of a twin crystal on the top {100} surface of a seed crystal to show how the morphology of the twin progresses with the alpha, beta, and gamma growth parameters. Conversely, it may be possible to experimentally determine these parameters from the morphology of the twinned crystal in the early stages of growth.

## 2. Principles of the model

### Notation:

3-dimensional vectors are in bold, e.g.  $\mathbf{r} = (r_x, r_y, r_z) = (r_1, r_2, r_3)$ .

Four-dimensional vectors have an arrow above them, e.g.  $\vec{\mathbf{r}} = (\mathbf{r}, l)$ .

The inner product of two vectors for any number of dimensions is

$$\langle \mathbf{x}, \mathbf{y} \rangle = \sum_i x_i y_i.$$

The norm of a vector is  $\|\mathbf{x}\| = \sqrt{\langle \mathbf{x}, \mathbf{x} \rangle}$ .

\* Corresponding author.

E-mail addresses: [a\\_bogatskiy@icloud.com](mailto:a_bogatskiy@icloud.com) (A. Bogatskiy), [jimbutler29@comcast.net](mailto:jimbutler29@comcast.net) (J.E. Butler).

## 2.1. Constructing the polyhedron

The geometric model assumes that there are four directions of growth in the diamond crystal which are normal to the four crystal faces enumerated with the following Miller indices: {100}, {110}, {111}, {113}. Taking all possible permutations and reflections of these vectors, we obtain 50 different growth vectors, collectively denoted as  $\langle 100 \rangle$ ,  $\langle 110 \rangle$ ,  $\langle 111 \rangle$ ,  $\langle 113 \rangle$ . Each of the vectors is normal to a plane that moves at a constant speed away from the origin (0,0,0) (“the  $\mathbf{n}$  plane”). For a dimensionless normal vector  $\mathbf{n}$ , call the corresponding speed  $V_{\mathbf{n}}$  (the velocity vector itself is  $V_{\mathbf{n}}\hat{\mathbf{n}}$  where  $\hat{\mathbf{n}}$  is the unit vector codirectional with  $\mathbf{n}$ ).

The crystal itself is a convex polyhedron  $P(t)$ , which is the intersection of all the negative half-spaces of the 50 planes (the negative half-space of a uniformly moving  $n$  plane at time  $t$  is the half-space covered by the plane over the time interval  $(-\infty, t)$ ).

As we will see later, the shape of the crystal depends only on the ratios of the speeds  $V_{100}$ ,  $V_{110}$ ,  $V_{111}$ ,  $V_{113}$ , hence the following reduced parameters are introduced:

$$\alpha = \frac{\sqrt{3}V_{100}}{V_{111}}, \beta = \frac{\sqrt{2}V_{100}}{V_{110}}, \gamma = \frac{\sqrt{11}V_{100}}{V_{113}}$$

If we introduce a more general and consistent notation of

$$\alpha_n = \frac{\|\mathbf{n}\| V_{100}}{V_n}$$

then  $\alpha = \alpha_{111}$ ,  $\beta = \alpha_{110}$  and  $\gamma = \alpha_{113}$ , whereas  $\alpha_{100} = 1$ . Note that  $V_n$  is invariant with respect to reflections and permutations of the axes. We shall further refer to  $\alpha_n$  as the *growth parameter of the  $n$  plane*.

The equation of the  $\mathbf{n}$  plane at time  $t$  is

$$\langle \mathbf{r}, \mathbf{n} \rangle = d_n l_0 + \|\mathbf{n}\| V_n t, \quad \mathbf{r} \in \mathbb{R}^3$$

where  $d_n$  is a dimensionless parameter which controls the initial position of the plane (at  $t = 0$ ) and  $l_0$  is taken to be the initial size of the crystal along the  $x$ -axis. In fact, the distance from the origin to the  $n$  plane at time  $t = 0$  is equal to  $\frac{d_n l_0}{\|\mathbf{n}\|}$ .

It is now natural to introduce dimensionless *normalized Cartesian coordinates*  $\hat{\mathbf{r}}$ , such that

$$\mathbf{r} = V_{100} t \hat{\mathbf{r}}.$$

Obviously, division by  $t$  is not practical in computer calculations, but using dimensionless coordinates makes sense in a theoretical treatment. Then the equation of the  $\mathbf{n}$  plane  $\pi_n$  becomes

$$\langle \hat{\mathbf{r}}, \mathbf{n} \rangle = d_n \frac{l_0}{V_{100} t} + \frac{\|\mathbf{n}\| V_n}{V_{100}},$$

which is equivalent to

$$\pi_n : \langle \hat{\mathbf{r}}, \mathbf{n} \rangle = \frac{2L d_n}{t} + \frac{\|\mathbf{n}\|^2}{\alpha_n},$$

where  $L = \frac{l_0}{2V_{100}}$ .

We see that the set of parameters  $L$ ,  $d_n$  and  $\alpha_n$  completely control the shape of the crystal at all times  $t$ , with  $L$  being the only parameter with dimensions ( $L$  controls the scaling of the time axis and the initial size of the crystal).

Computationally, the easiest way to specify a plane is by providing its normal vector  $\mathbf{n}$  and the point on that plane closest to the origin, which is the intersection of the plane with the straight line going along  $\mathbf{n}$ . Suppose

that this point is

$$\hat{\mathbf{r}}_n = \frac{1}{p_n} \mathbf{n}.$$

Then, from the equation of the plane,

$$p_n = \frac{t}{\frac{2L d_n}{\|\mathbf{n}\|^2} + \frac{t}{\alpha_n}}.$$

Note that, although this formula does not look very simple, these parameters are natural because

$$\lim_{t \rightarrow \infty} p_n = \alpha_n.$$

The numbers  $p_n$  are the *effective values of the growth parameters*  $\alpha_n$  at finite times. The same observation proves that the shape of the crystal stabilizes at large times and is determined solely by the parameters  $\alpha_{110}$ ,  $\alpha_{111}$  and  $\alpha_{113}$ . Moreover, independent of the initial shape of the crystal, its shape at infinite time is always completely symmetrical (with respect to reflections and permutations of the axes), assuming that growth in all directions is allowed.

Finally, the initial shape of the crystal is determined by the 50 parameters  $d_n$ . When the initial shape of the crystal contains only some of the 50 possible faces, the remaining planes have undefined values of  $d_n$ . From the perspective of crystal growth, it is natural to take such values of  $d_n$  that the corresponding planes are *tangent* to the initial polyhedron.

Since the slightly more convenient way of specifying a plane is to specify any one of its points, we need a way to calculate  $d_n$  from that data. Say, we know that the plane  $\pi_n$  contains a point  $\mathbf{r} = l_0 \mathbf{v}_n$  at  $t = 0$ . Then, from the equation of the plane, we have

$$d_n = \langle \mathbf{v}_n, \mathbf{n} \rangle.$$

The equation of the  $\mathbf{n}$  plane for  $t > 0$  is then

$$\pi_n : \langle \hat{\mathbf{r}}, \mathbf{n} \rangle = \frac{2L}{t} \langle \mathbf{v}_n, \mathbf{n} \rangle + \frac{\|\mathbf{n}\|^2}{\alpha_n},$$

which, when combined with our definition of  $p_n$ , is equivalent to

$$\pi_n : \langle \hat{\mathbf{r}}, \mathbf{n} \rangle = \frac{\|\mathbf{n}\|^2}{p_n}.$$

In order to make the equations even simpler, we introduce the following 4-dimensional vectors, as is usually done in computational geometry. Instead of  $\hat{\mathbf{r}} = (\hat{x}, \hat{y}, \hat{z})$ , we take

$$\vec{\mathbf{r}} = (\hat{x}, \hat{y}, \hat{z}, l) = (\mathbf{r}, l)$$

and instead of  $\mathbf{n}$  and  $p_n$  take

$$\vec{\mathbf{n}} = \left( n_x, n_y, n_z, -\frac{\|\mathbf{n}\|^2}{p_n} \right) = \left( \mathbf{n}, -\frac{\|\mathbf{n}\|^2}{p_n} \right).$$

Then the equation of the  $n$  plane is

$$\pi_n : \langle \vec{\mathbf{r}}, \vec{\mathbf{n}} \rangle = 0.$$

Moreover, the negative half-space  $P_n^-$  is precisely the set of all the points  $\vec{\mathbf{r}} = (\hat{\mathbf{r}}, l)$  that satisfy the inequality

$$P_n^- : \langle \vec{\mathbf{r}}, \vec{\mathbf{n}} \rangle \leq 0.$$

This is the preferred form of these relations when computing in Mathematica.

To find the vertices of the polyhedron that is the intersection  $P(t) = \cap_n P_n(t)$ , one has to find all the intersections of all the 3-tuples of the planes  $\pi_n$  and select only those points that satisfy the last inequality for all vectors  $\mathbf{n}$ .

## 2.2. Vicinal surfaces

Each of the  $\mathbf{n}$  planes can be chosen to be a “vicinal cut”, i.e. a slightly tilted plane relative to the original normal vector  $\mathbf{n}$ . In our model, such an inclination is described by two angles,  $0 < \theta < \pi$  and  $0 \leq \varphi < 2\pi$ , which correspond to the standard spherical angles in a reference frame where  $\mathbf{n}$  is directed along the  $z$ -axis. The angle  $\theta$  is generally restricted to small values of no more than a few degrees. Let us call the tilted normal vector  $\mathbf{n}_{\theta, \varphi}$ . According to the experimental data, such faces of a crystal can grow at a somewhat higher speed than  $V_n$ . Therefore we include in our model four additional parameters  $m_n > 1$  for  $\mathbf{n} = (100)$ ,  $(110)$ ,  $(111)$ ,  $(113)$ , called “vicinal cut speed multipliers”, defined through

$$V_{n_{\theta, \varphi}} = m_n V_n.$$

After setting the angles of all the vicinal surfaces, one can specify the initial shape of the crystal using the same parameters  $d_{n_{\theta, \varphi}}$ , which describe the distance of a given plane to the origin. The original  $\mathbf{n}$  planes are automatically moved so that they are tangent to the initial polyhedron at  $t = 0$ . After some finite time, all the vicinal surfaces are “outgrown” by the  $n$  planes (assuming that the values of  $\theta$  are small enough).

## 2.3. Growth parameters changing with time

### 2.3.1. Naive approach

Suppose that the growth speeds  $V_n$  change with time. Then put

$$\alpha_n = \frac{\|\mathbf{n}\| V_{100}(0)}{V_n(t)}.$$

The initial equation of the  $\mathbf{n}$  plane becomes simply

$$\langle \mathbf{r}, \mathbf{n} \rangle = d_n l_0 + \|\mathbf{n}\| \int_0^t V_n(\tau) d\tau.$$

After we introduce new coordinates  $\mathbf{r} = V_{100}(0)t\hat{\mathbf{r}}$  and  $L = \frac{l_0}{2V_{100}(0)}$  this becomes

$$\langle \hat{\mathbf{r}}, \mathbf{n} \rangle = \frac{2Ld_n}{t} + \frac{\|\mathbf{n}\|^2}{t} \int_0^t \frac{1}{\alpha_n(\tau)} d\tau.$$

Comparing this with  $\langle \hat{\mathbf{r}}, \mathbf{n} \rangle = \frac{\|\mathbf{n}\|^2}{p_n}$  we find that

$$p_n = t \left( \frac{2Ld_n}{\|\mathbf{n}\|^2} + \int_0^t \frac{1}{\alpha_n(\tau)} d\tau \right)^{-1}.$$

Once again, if there is a limit

$$\lim_{t \rightarrow \infty} \alpha_n = \alpha_n(\infty) > 0,$$

then

$$\lim_{t \rightarrow \infty} p_n = \alpha_n(\infty).$$

Like before, the equations of the planes are

$$\pi_n : \langle \hat{\mathbf{r}}, \mathbf{n} \rangle = \frac{\|\mathbf{n}\|^2}{p_n}.$$

### 2.3.2. System of integral equations

Unfortunately, the “naive” derivation performed above is not very useful in the computational model described earlier. The problem is that after *each change* of the growth parameters all planes need to be moved so that they are tangent to the polyhedron  $P(t)$  (a plane is left invariant by this transformation if it already produces a face of  $P(t)$ ). And if the parameters are changing continuously, this turns the system of (at most) 50 independent algebraic equations into a system of 50 intertwined “integro-differential procedures”, where the calculation of  $P(t)$  requires the knowledge of its history over some past time interval  $(t - \delta t, t)$ .

More precisely, for the polyhedron  $P(t)$ , define  $\mathbf{w}_n(P(t))$  as a vertex of  $P(t)$  that is closest to the plane  $\pi_n(t)$  (and thus lies in that plane). Then the instantaneous velocity of this vertex is completely determined by the three faces it belongs to. Let us call the normal vectors of these faces  $\mathbf{n}_i = (n_{ix}, n_{iy}, n_{iz})$ ,  $i = 1, 2, 3$  (keep in mind the dependence of these on  $\mathbf{n}$ ). Note that, in general, the set of vectors  $\mathbf{n}_i$  for a given plane  $\pi_n$  changes with time. Then the velocity vector  $\mathbf{V}(P(t); \mathbf{n}, t) = (u_1, u_2, u_3)$  of the point  $\mathbf{w}_n$ , which depends on time *explicitly* through the speeds  $V_{n_i}(t)$  as well as *implicitly* through the shape of  $P(t)$ , is the unique solution of the simple linear system

$$\begin{pmatrix} n_{1x} & n_{1y} & n_{1z} \\ n_{2x} & n_{2y} & n_{2z} \\ n_{3x} & n_{3y} & n_{3z} \end{pmatrix} \begin{pmatrix} u_1 \\ u_2 \\ u_3 \end{pmatrix} = \begin{pmatrix} \|\mathbf{n}_1\|^2 V_{n_1}(t) \\ \|\mathbf{n}_2\|^2 V_{n_2}(t) \\ \|\mathbf{n}_3\|^2 V_{n_3}(t) \end{pmatrix}.$$

If we denote the matrix on the left-hand side by  $N(P(t); \mathbf{n})$ , then

$$\frac{\mathbf{V}(P(t); \mathbf{n}, t)}{V_{100}(0)} = N(P(t); \mathbf{n})^{-1} \begin{pmatrix} \|\mathbf{n}_1\|^2 / \alpha_{n_1}(t) \\ \|\mathbf{n}_2\|^2 / \alpha_{n_2}(t) \\ \|\mathbf{n}_3\|^2 / \alpha_{n_3}(t) \end{pmatrix}.$$

Since there is only a finite number of possible combinations of normal vectors  $\mathbf{n}_i$ , the speed  $\mathbf{V}$  is always expressed in terms of  $\alpha_{n_i}(t)$  in one of a finite number of ways. If the projection of  $\mathbf{V}(P(t); \mathbf{n}, t)$  on the  $\mathbf{n}$  direction is less than  $V_n(t)$ , then the  $\mathbf{n}$  plane has to move along with the vertex  $\mathbf{w}_n$ . Otherwise, the  $\mathbf{n}$  plane starts producing a new face, thus, “splitting” the old vertex  $\mathbf{w}_n$  into several new vertices, whose speed along  $\mathbf{n}$  is equal to  $V_n(t)$ . With this in mind,

$$\langle \mathbf{r}, \mathbf{n} \rangle = d_n l_0 + \int_0^t \min\{\langle \mathbf{V}(P(\tau); \mathbf{n}, \tau), \mathbf{n} \rangle, \|\mathbf{n}\| V_n(\tau)\} d\tau,$$

which is equivalent to

$$\pi_n : \langle \hat{\mathbf{r}}, \mathbf{n} \rangle = \frac{2Ld_n}{t} + \frac{1}{t} \int_0^t \min\left\{ \left\langle \frac{\mathbf{V}(P(\tau); \mathbf{n}, \tau)}{V_{100}(0)}, \mathbf{n} \right\rangle, \frac{\|\mathbf{n}\|^2}{\alpha_n(\tau)} \right\} d\tau.$$

Obviously, this equation of the  $\mathbf{n}$  plane requires knowledge of the whole history of  $P(\tau)$ , i.e. of all the planes  $\pi_n(\tau)$ , for  $\tau < t$ . From the mathematical point of view, this is a system of integral equations on  $\langle \hat{\mathbf{r}}, \mathbf{n} \rangle(t)$  for all  $\mathbf{n}$ . Alas, the extremely implicit form of the equations makes it very difficult to analyze them or even suggest a computational method of solving them.

The simplest example of such behavior is when  $\mathbf{V}_n$  are piecewise constant functions of time. Put  $t_0 = 0$  and suppose that  $t_i$  for  $i = 1, 2, \dots$  are the points of jumps for all the functions  $\mathbf{V}_n(t)$  and hence  $\alpha_n(t)$ . Then we would only have to find the minimum in (3) for  $t = t_i$ , i.e. the integrand in (3) is piecewise constant on the same intervals. In fact, the evolution of the crystal  $P(t)$  between the jump points  $t_i$  is correctly described by the equations of the form (1): at each point  $t_i$ , the constructed polyhedron  $P(t_i)$  is taken to be the initial polyhedron for the next evolution interval  $(t_i, t_{i+1})$  with the new values of the growth parameters.

### 3. Implementation of the model

#### 3.1. Software

The model was implemented using Wolfram Mathematica version 9 to create an executable CDF file, **DCVDVicinal.cdf**, which can be used with Wolfram CDF reader (version 9.0.1.0, free download). The cubic initial shape implies that each of the 50 planes has to include at least one of the vertices of the cube with side  $l_0$ , i.e. the eight points  $\frac{l_0}{2}(1, 1, 1)$ ,  $\frac{l_0}{2}(-1, 1, 1)$ , ...,  $\frac{l_0}{2}(-1, -1, -1)$ . Therefore  $d_n = \frac{1}{2}(n_x + n_y + n_z)$  with  $\mathbf{n} = (n_x, n_y, n_z)$ . The values of  $p_n$  are found from the condition that  $\hat{\mathbf{r}}_n$  lie in  $\pi_n$ :

$$p_{100} = \frac{t}{L+t}, p_{110} = \frac{t}{L+\frac{t}{\alpha_{110}}}, p_{111} = \frac{t}{L+\frac{t}{\alpha_{111}}}, p_{113} = \frac{t}{\frac{5}{11}L+\frac{t}{\alpha_{113}}}$$

Upon initialization of the CDF file, you are presented with three main interactive areas: the 3D model, the type diagram and the 2D section view. The two latter areas are fully integrated into the first one, thus will not need a detailed description.

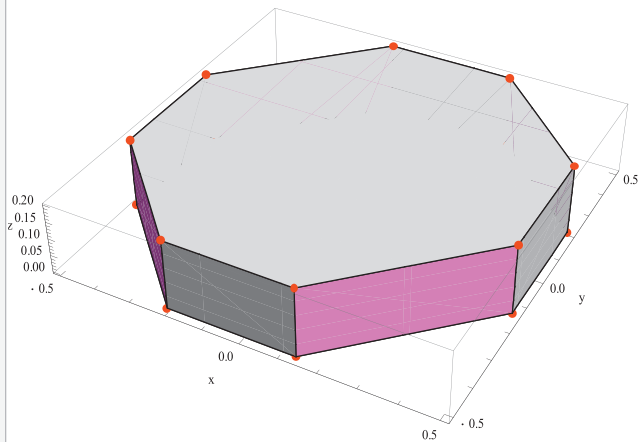
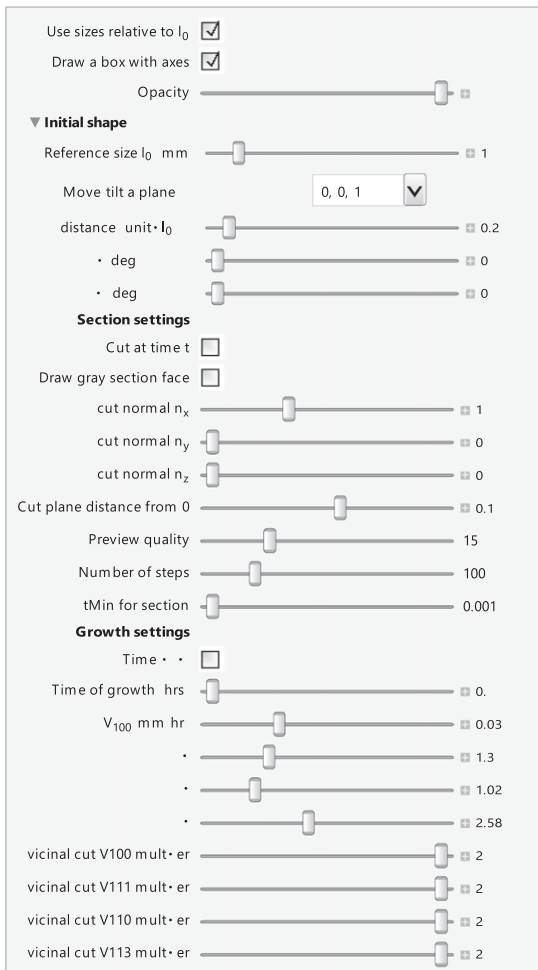
When the initial polyhedron  $P(0)$  is not a cube, only a little modification to the algorithm is needed. However, all the computations become significantly slower due to reduced symmetry.

The main difference from the cubic case is that now we have to find a way to automatically find such values of  $d_n$  that all the planes are tangent to the initial polyhedron (at least at  $t = 0$ ). To do that, for each  $\mathbf{n}$  simply find a vertex  $\mathbf{v}$  of  $P(0)$  closest to the  $\mathbf{n}$  plane, i.e. which minimizes the value of  $|\langle \mathbf{v}, \mathbf{n} \rangle|$ . Then reset the value of  $d_n$  to  $\langle \mathbf{v}, \mathbf{n} \rangle$ .

#### 3.2. Interface

When you open the CDF file, the initial 3D view is an orthogonal projection along the z axis. This is displayed in Fig. 1. You can rotate the graphics interactively at any time with the mouse pointer on the right hand side of the screen holding down the left button. Values of the parameters that are controlled by sliders on the left side of the screen and values can be entered manually by clicking the tiny “+” button to the right of the corresponding slider. There is a general zoom control in the bottom right corner of the window. If the setting “Use sizes relative to  $l_0$ ” is turned on, the coordinates of the points shown in the Mathematica 3D model at finite times are

$$\frac{t\hat{\mathbf{r}}}{2L} = \frac{\mathbf{r}}{l_0}$$



Sizes are relative to  $l_0$ .  
Type: 100 110  
10 Faces, 24 Edges, 16 Vertices.

Fig. 1. An example of the cdf interface window.

i.e. relative to  $l_0$ . The setting “Draw a box with axes” enables the framed interface for the 3D model. The “Opacity” slider controls the transparency of the faces of the polyhedron (note that it does not change the transparency of the section face and growth sectors on it). Next, we outline the main controls available on the left side of the simulation interface.

### 3.2.1. Initial shape

The initial shape of the single crystal seed can be designed by the controls on the left side of the screen. “Reference size  $l_0$  (mm)” sets a distance in millimeters, which is then used in the calculations instead of  $l_0$ , as outlined in the first section. It is recommended that the size of the substrate does not exceed  $2 l_0$ .

“Move/tilt a plane” lets you choose any of the moving planes  $\pi_{\mathbf{n}}$  (0) at time  $t = 0$ . The following three sliders control the initial position and inclination of these planes with respect to their normal vectors.

“Distance (unit =  $l_0$ )” sets the distance from the origin to the plane  $\pi_{\mathbf{n}}$  at  $t = 0$ . Values relative to  $l_0$  are used so that the initial shape is independent of  $l_0$ .

“ $\theta$  (deg)” and “ $\varphi$  (deg)” are the two standard spherical angles of the coordinate system in which the  $z$ -axis is directed along  $\mathbf{n}$ . Introducing a nonzero  $\theta$ , one can specify a vicinal face associated with  $\mathbf{n}$ . Note that for the vicinal surfaces, the “Distance (unit =  $l_0$ )” slider specifies the distance from the origin to the new *inclined* plane.

Fig. 2 displays several examples of initial seed shapes.

“Opacity” controls the transparency of the faces of the polyhedron.

### 3.2.2. Growth settings

“ $t = \infty$ ” sets the time to infinity and the polyhedron shown on the right-hand side is the ultimate shape.

“Time of growth (hrs)” sets the time  $t$  in hours at which the polyhedron  $P(t)$  is calculated.

“ $V_{100}$  (mm/h)” sets the value of the growth speed  $V_{100}$  in millimeters per hour.

“ $\alpha$ ”, “ $\beta$ ”, “ $\gamma$ ” are the three main growth parameters defined in the first section.

The four sliders “Vicinal cut  $Vn$  multiplier” control the multipliers  $m_{\mathbf{n}}$  for  $\mathbf{n} = (100)$ ,  $(110)$ ,  $(111)$ ,  $(113)$  as described in Subsection 2.2.

Fig. 3 displays an example of the evolution of the growth for a particular seed shape and growth parameter settings.

### 3.2.3. Section settings

It is possible to view the growth sectors inside the crystal in the form of their traces on the section pane

$$x = l_0 c.$$

Note that each section comprises many thin colored polygons, therefore it may appear transparent if their number is too low. Each of the polygons is the section of the polyhedron  $P(\tau)$  at some point in time  $\tau$  between 0 and  $t$  with its edges colored in agreement with the colors of the faces they were in. Note that there is always *equal amount of time* between two neighboring polygons. There may be a hole in the middle of the section. It corresponds to the case when the section plane has a normal vector which coincides with one of the normal vectors of the polyhedron and thus the corresponding face of the crystal “hits” the section plane at some positive time  $t_0$ , therefore giving the nonzero size of the earliest nonempty section.

The “Cut at time  $t$ ” checkbox enables the section mode.

The “Draw gray section face” checkbox controls the visibility of the gray face that is drawn behind the section polygons. Enabling this option is recommended if the section plane looks transparent and you do not want to increase the number of polygons. With this setting on it is recommended to turn up the “Opacity” setting to 1 to avoid clipping.

The three sliders “Cut normal  $n_{x,y,z}$ ” specify the normal vector of the cutting plane.

“Cut plane distance from 0” changes the position of the cutting plane.

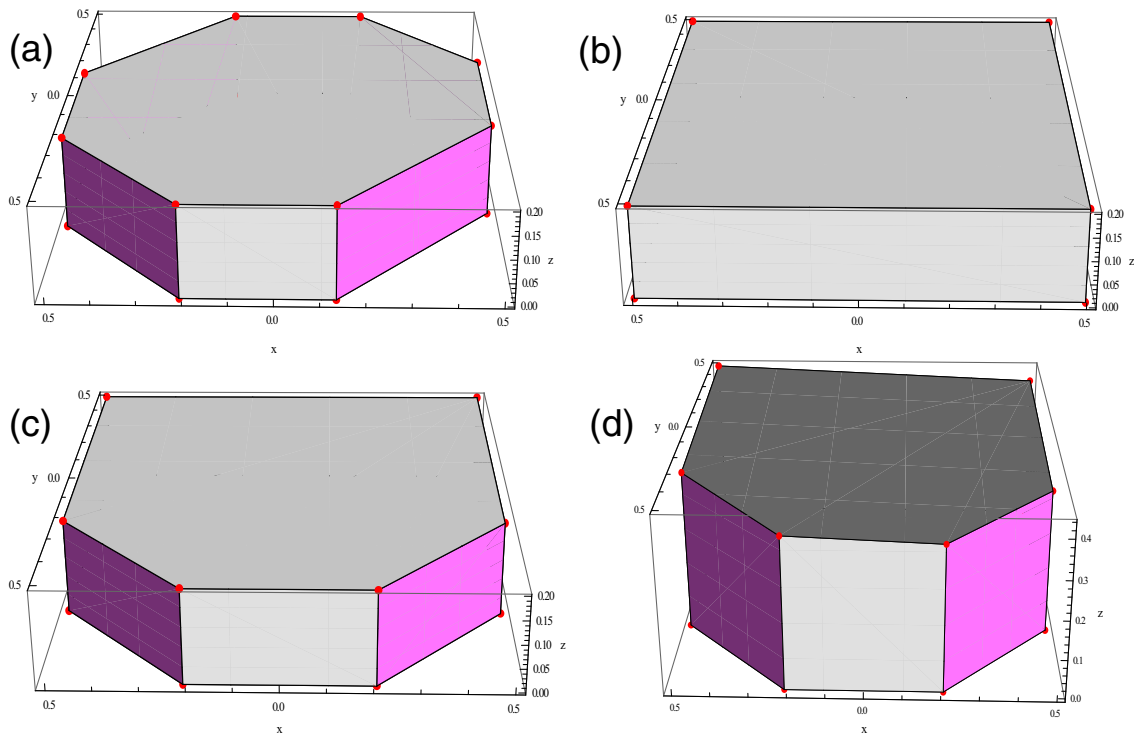
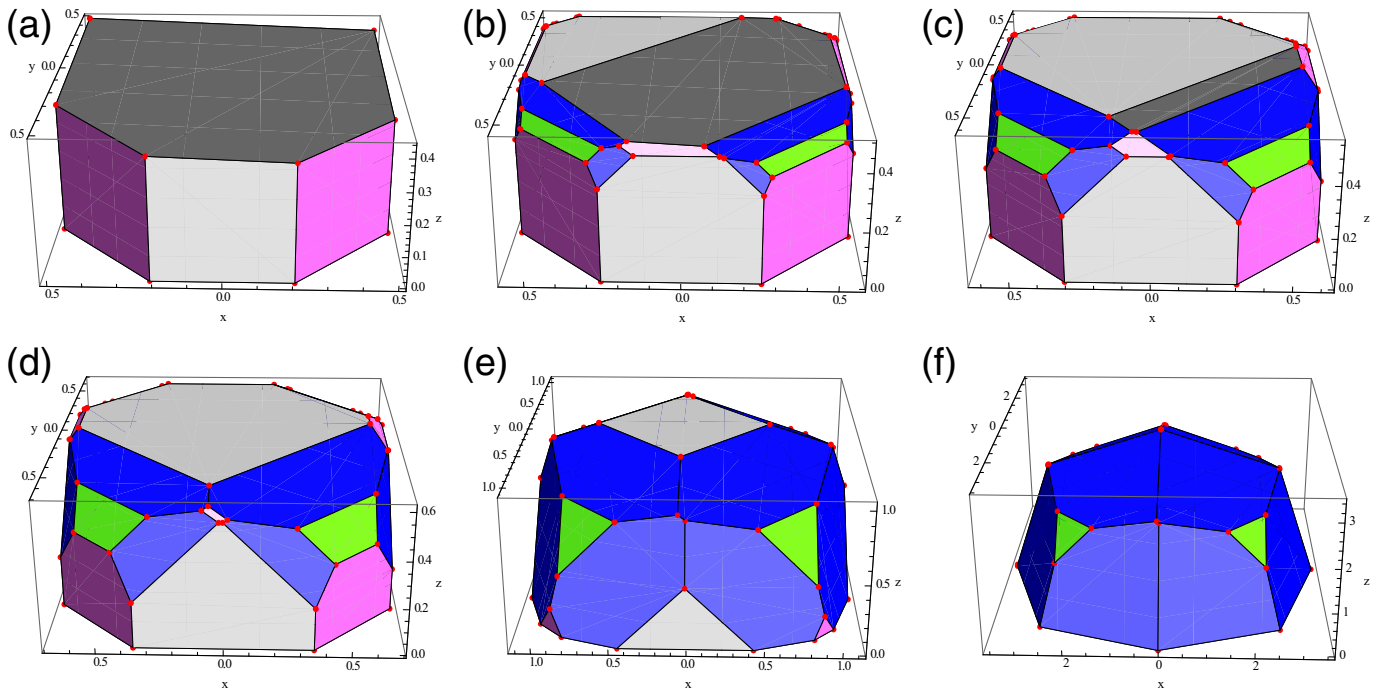


Fig. 2. (a) Top gray face (001), bounded on the sides by gray (100), (010), (-100), (0-10), and pink (110), (1-10), (-110), (-1-10); (b) top gray face (001), bounded on the sides by gray (100), (010), (-100), (0-10); (c) top gray face (001), bounded on the sides by gray (100), (010), (-100), (0-10), and pink (1-10), (-1-10); (d) vicinal off axis top face 3° off (001) in the direction of (1-10), bounded on the sides by gray (100), (010), (-100), (0-10), and pink (1-10), (-1-10).



**Fig. 3.** Evolution of the seed shown in Fig. 2(d) for  $\alpha = 1.9$ ,  $\beta = 1.1$ ,  $\gamma = 4$ , growth rate  $30 \mu\text{m}$  per hour, vicinal cut  $V_{100}$  multiplier of 1.4, and for growth times of (a) 0 h, (b) 2 h, (c) 4 h, (d) 6 h, (e) 20 h, and (f) 100 h.

“Preview quality” sets the number  $N_0$  of section polygons that are drawn *while* the control sliders are being dragged.

“Number of steps” sets the number  $N$  of section polygons that are drawn *after* all the control sliders are released. While this slider is dragged, the 3D model is not updated interactively. Note that choosing high values of  $N$  can dramatically increase the render time of the model after any change is made to the growth parameters.

“tMin for section” sets the moment  $t_{min}$  such that the interval  $(t_{min}, t)$  is divided into  $N$  (or  $N_0$ ) equal segments and there is one section polygon calculated for each of the segments (including the empty sections).

Fig. 4 displays examples of sections thru the grown crystal.

#### 4. Twin morphology

This section will explore the morphology of a twinned crystal nucleating on a  $\{100\}$  surface, a ‘penetration twin’. The development of the morphology of a twin in a diamond crystal is implemented in a separate CDF model, DCVDtwin.cdf. In this model, a twin is nucleated on the  $(100)$  surface, and then all the exterior surfaces of the twin and original seed are evolved according to the alpha, beta, and gamma growth parameters. A twin can form on a  $100$  face of the crystal and grow from zero size as an independent completely symmetric crystal. The axes of this crystal are rotated through  $60^\circ$  about the  $111$  axis. The center of the twin can

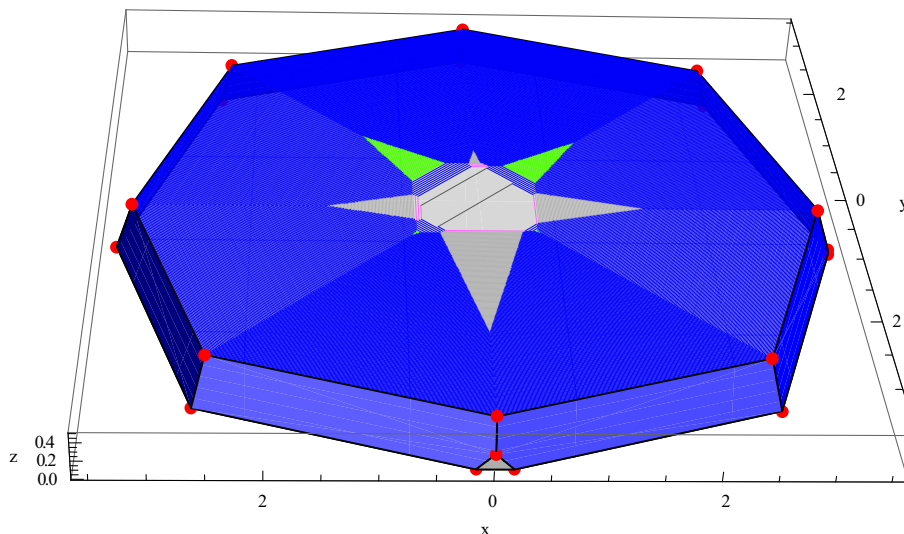


**Fig. 4.** A cut through the crystal of Fig. 3(f), normal to  $(001)$  at a distance of 0.5 from the origin showing various growth sectors.

be positioned at any point  $(x, y, z)$  with the help of the corresponding sliders.

The twin is stable (is not overgrown by the parent crystal) on a  $\{100\}$  if and only if the following conditions are met

$$\left\{ \begin{array}{l} 0 < \alpha \leq \frac{5}{3} \\ 0 < \beta \leq \frac{5}{3} \\ 0 < \gamma \leq \frac{11}{3} \end{array} \right., \text{ or } \left\{ \begin{array}{l} \frac{5}{3} < \alpha \leq 2 \\ 0 < \beta \leq \frac{2\alpha}{3(\alpha-1)} \\ 0 < \gamma \leq \frac{11}{3} \end{array} \right.$$

These conditions were determined analytically by finding all the points of intersection among all the planes and analyzing when each of them is a vertex of the twin and its speed in the appropriate direction is more than  $V_{100}$ .

The main limitation of our model is that the twin has to be sufficiently far away from other faces of the main crystal at all times. Otherwise, the

model acquires an inherent non-convexity, which cannot be accounted for by the computational methods used in the model.

It is important to note that the original conditions for the stability of a penetration twin on a  $\{100\}$  surface [8,9],  $\alpha < 2$ , was determined in models only considering  $\{100\}$  and  $\{111\}$  surfaces, and now needs to be modified to the conditions above. This can now explain the observation of the lack of penetration twins in homoepitaxial single growth when  $\alpha = 1.8$  (Fig. 1 in ref. [12]).

Experimentally, the values reported for  $\alpha$ ,  $\beta$ , and  $\gamma$  in microwave plasma CVD of single crystal diamond growth are in the range [11–13,20]

$$1.5 \leq \alpha \leq 2.5$$

$$0.8 \leq \beta \leq 1.1$$

$$3 \leq \gamma \leq 7.1.$$

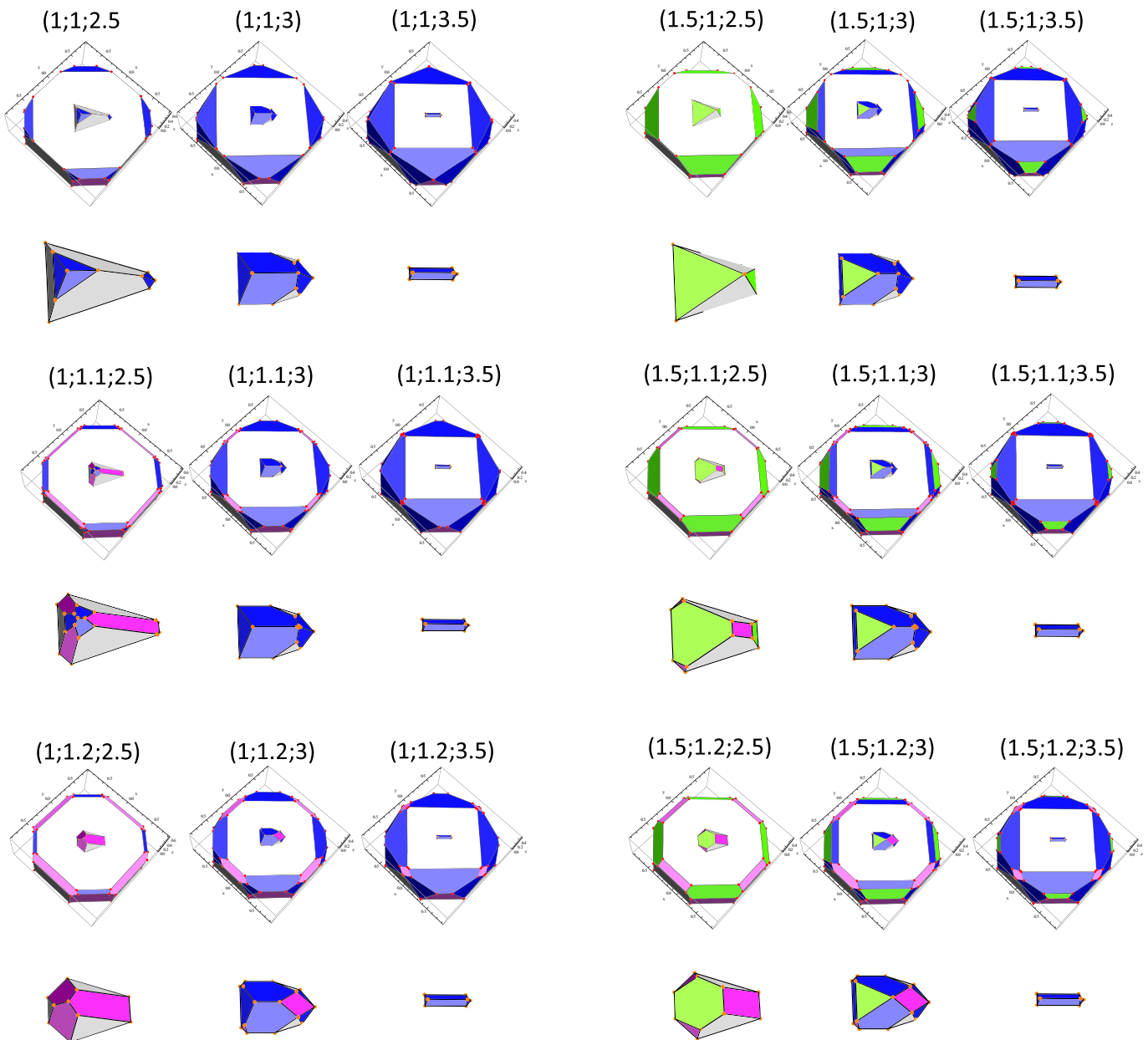


Fig. 5. Examples of the morphology of penetration twins on the 100 surface as a function of  $(\alpha; \beta; \gamma)$  for some values of the parameters typical of microwave plasma CVD single crystal diamond growth.

We present in Fig. 5 the morphology of an isolated penetration twin on the {100} surface for a few values of  $\alpha$ ,  $\beta$ , and  $\gamma$  in the range listed above.

We have also analytically determined the stability conditions for a penetration twin growing on a {111} surface in the same manner used above. The conditions for a stable penetration twin on a {111} surface are:

$$\begin{cases} \frac{3}{2} \leq \alpha \leq \frac{9}{5} \\ 0 \leq \beta \leq \frac{4\alpha}{9-3\alpha} \\ 0 \leq \gamma \leq \frac{11\alpha}{9-2\alpha} \end{cases}, \quad \text{or} \quad \begin{cases} \alpha \geq \frac{9}{5} \\ 0 \leq \beta \leq \frac{10\alpha}{9} \\ 0 \leq \gamma \leq \frac{55\alpha}{27} \end{cases}$$

And for a contact twin on a {111}, the conditions are the same as for the existence of {111} surfaces:

$$\alpha \geq 1$$

$$0 \leq \beta \leq \alpha$$

$$0 \leq \gamma \leq \frac{11}{5} \alpha$$

We have not yet implemented a specific cdf program to show the morphology of the penetration twin on {111}, but hopefully this will be available by the time of publication.

## 5. Conclusion

A geometric model of growth of a cubic crystal has been implemented in readily available software. New conditions for the stability of penetration twins on {100} and {111} surfaces have been determined.

Such modeling has value in designing growth conditions optimized to particular properties. For example, the incorporation of impurities, dopants, and the formation of structural defects depends on the local surface structure. Each of the low index planes in the model has a different stereochemical structure and thus the bulk material grown under a particular low index surface (often referred to as the ‘growth sector’) will have different physical properties reflecting the local defects and impurities in the growth sector. For example, the  $\langle 111 \rangle$  growth sectors in CVD grown diamond materials show high dislocation densities [18, 19], twin formation [16,17], and impurities such as phosphorous incorporation [21]. The  $\langle 110 \rangle$  growth sectors are reported to have high stress [14]. These differing physical properties can cause strain, cracking, color and wear gradations, and variations in a host of other physical properties. Hence, knowledge of the impact of the alpha, beta, and gamma growth parameters on the growth morphology by using growth modeling, is useful in selecting the growth conditions for the desired product.

## Prime novelty statement

A geometric model of cubic crystal growth based on the relative growth velocities of the {100}, {110}, {111}, and {113} crystal planes is implemented in a readily available (free) software. The mathematical foundation for the models is provided and implemented in two programs. The first, DCVDVicinal.cdf, presents the evolving morphology of crystal growth from a seed bounded by {100}, {110}, {111} and/or {113} planes and includes the option for a vicinal (off axis) surface. The second, DCVDtwin.cdf, presents the evolution of a twin formed on the surface of a {100} plane. New conditions for the stability of penetration twins on {100} and {111} surfaces in terms of the alpha, beta, and gamma growth parameters are presented.

## Acknowledgments

Dr. Alexander Altmark is thanked for enlightening discussions. This work was supported by Act 220 of the Russian Government (Agreement No.14B25.31.0021 with the host organization IAPRAS).

## Appendix A

Supplementary data to this article can be found online at <http://dx.doi.org/10.1016/j.diamond.2014.12.010>.

## References

- [1] S. Matsumoto, Y. Sato, M. Kamo, N. Setaka, Vapor-deposition of diamond particles from methane, *Jpn. J. Appl. Phys. 2 Lett.* 21 (1982) L183–L185.
- [2] C. Wild, N. Herres, P. Koidl, Texture formation in polycrystalline diamond films, *J. Appl. Phys.* 68 (1990) 973–978.
- [3] W.J.P. Vannekevort, G. Janssen, L.J. Giling, Anisotropy in monocrystalline CVD diamond growth. I. A sphere growth experiment, *J. Cryst. Growth* 113 (1991) 295–304.
- [4] G. Janssen, J.J. Schermer, W.J.P. Vannekevort, L.J. Giling, On the occurrence of (113) facets on CVD-grown diamond, *J. Cryst. Growth* 125 (1992) 42–50.
- [5] K.A. Snail, Z.P. Lu, R. Weimer, J. Heberlein, E. Pfender, L.M. Hanssen, Confirmation of (113) facets on diamond grown by chemical-vapor-deposition, *J. Cryst. Growth* 137 (1994) 676–679.
- [6] J.E. Butler, R.L. Woodin, Thin-film diamond growth mechanisms, *Philos. Trans. R. Soc. A Math. Phys. Eng. Sci.* 342 (1993) 209–224.
- [7] J.E. Butler, Y.A. Mankelevich, A. Cheesman, J. Ma, M.N.R. Ashfold, Understanding the chemical vapor deposition of diamond: recent progress, *J. Phys. Condens. Matter* 21 (2009).
- [8] C. Wild, R. Kohl, N. Herres, W. Mullerseberr, P. Koidl, Oriented CVD diamond films – twin formation, structure and morphology, *Diam. Relat. Mater.* 3 (1994) 373–381.
- [9] M.A. Tamor, M.P. Everson, On the role of penetration twins in the morphological development of vapor-grown diamond films, *J. Mater. Res.* 9 (1994) 1839–1848.
- [10] F. Silva, J. Achard, X. Bonnin, A. Michau, A. Tallaire, O. Brinza, A. Gicquel, 3D crystal growth model for understanding the role of plasma pre-treatment on CVD diamond crystal shape, *Phys. Status Solidi A Appl. Mater. Sci.* 203 (2006) 3049–3055.
- [11] O. Brinza, J. Achard, F. Silva, X. Bonnin, P. Barroy, K. De Corte, A. Gicquel, Dependence of CVD diamond growth rate on substrate orientation as a function of process parameters in the high microwave power density regime, *Phys. Status Solidi A Appl. Mater. Sci.* 205 (2008) 2114–2120.
- [12] F. Silva, X. Bonnin, J. Achard, O. Brinza, A. Michau, A. Gicquel, Geometric modeling of homoepitaxial CVD diamond growth: I. The {100}{111}{110}{113} system, *J. Cryst. Growth* 310 (2008) 187–203.
- [13] F. Silva, J. Achard, X. Bonnin, O. Brinza, A. Michau, A. Secroun, K. De Corte, S. Felton, M. Newton, A. Gicquel, Single crystal CVD diamond growth strategy by the use of a 3D geometrical model: growth on (113) oriented substrates, *Diam. Relat. Mater.* 17 (2008) 1067–1075.
- [14] R. Issaoui, J. Achard, F. Silva, A. Tallaire, V. Mille, A. Gicquel, Influence of oxygen addition on the crystal shape of CVD boron doped diamond, *Phys. Status Solidi A Appl. Mater. Sci.* 208 (2011) 2023–2027.
- [15] A. Tallaire, J. Achard, F. Silva, O. Brinza, A. Gicquel, Growth of large size diamond single crystals by plasma assisted chemical vapour deposition: recent achievements and remaining challenges, *C. R. Phys.* 14 (2013) 169–184.
- [16] T. Tsuno, T. Imai, N. Fujimori, Twinning structure and growth hillock on diamond (001) epitaxial film, *Jpn. J. Appl. Phys. 1 Regul. Pap. Short Notes Rev. Pap.* 33 (1994) 4039–4043.
- [17] J.E. Butler, I. Oleynik, A mechanism for crystal twinning in the growth of diamond by chemical vapour deposition, *Philos. Trans. R. Soc. A Math. Phys. Eng. Sci.* 366 (2008) 295–310.
- [18] N.C. Burton, J.E. Butler, A.R. Lang, J.W. Steeds, On a characteristic misorientation structure within (001) facets of CVD-grown diamond crystallites – an analysis by optical microtopography, interferometry, electron-diffraction and cathodoluminescence, *Proc. R. Soc. Lond. A Math. Phys. Sci.* 449 (1995) 555–566.
- [19] J.W. Steeds, A. Gilmore, J.A. Wilson, J.E. Butler, On the nature of extended defects in CVD diamond and the origin of compressive stresses, *Diam. Relat. Mater.* 7 (1998) 1437–1450.
- [20] A. Tallaire, J. Achard, O. Brinza, V. Mille, M. Naamoun, F. Silva, A. Gicquel, Growth strategy for controlling dislocation densities and crystal morphologies of single crystal diamond by using pyramidal-shape substrates, *Diam. Relat. Mater.* 33 (2013) 71–77.
- [21] S. Koizumi, M. Kamo, Y. Sato, H. Ozaki, T. Inuzuka, Growth and characterization of phosphorous doped {111} homoepitaxial diamond thin films, *Appl. Phys. Lett.* 71 (1997) 1065–1067.